Article

Anion Influence on Spin State in Two Novel Fe(III) Compounds: [Fe(5F-sal$_2$333)]X

Sriram Sundaresan [1], Irina A. Kühne [1,2], Conor T. Kelly [1], Andrew Barker [1], Daniel Salley [1], Helge Müller-Bunz [1], Annie K. Powell [2,3] and Grace G. Morgan [1,*]

[1] Centre for Synthesis and Chemical Biology, School of Chemistry and Chemical Biology, University College Dublin (UCD), Belfield, Dublin 4, Ireland; sriram.sundaresan@ucdconnect.ie (S.S.); irina.kuhne@ucd.ie (I.A.K.); conor.kelly@ucdconnect.ie (C.T.K.); andrew.barker@ucdconnect.ie (A.B.); danielsalley1@gmail.com (D.S.); helge.muellerbunz@ucd.ie (H.M.-B.)

[2] Institute for Inorganic Chemistry (AOC), KIT (Karlsruhe Institute of Technology), Engessterstr. 15, 76131 Karlsruhe, Germany; annie.powell@kit.edu

[3] Institute for Nanotechnology (INT), KIT (Karlsruhe Institute of Technology), Hermann-von-Helmholtz-Platz 1, 76344 Eggenstein-Leopoldshafen, Germany

* Correspondence: grace.morgan@ucd.ie; Tel.: +353-1-716-2295

check for updates

Abstract: Structural and magnetic data on two iron (III) complexes with a hexadentate Schiff base chelating ligand and Cl^- or BPh_4^- counterions are reported. In the solid state, the Cl^- complex [Fe(5F-sal$_2$333)]Cl, **1**, is high spin between 5–300 K while the BPh_4^- analogue [Fe(5F-sal$_2$333)]BPh$_4$, **2**, is low spin between 5–250 K, with onset of a gradual and incomplete spin crossover on warming to room temperature. Structural investigation reveals different orientations of the hydrogen atoms on the secondary amine donors in the two salts of the [Fe(5F-sal$_2$333)]$^+$ cation: high spin complex [Fe(5F-sal$_2$333)]Cl, **1**, crystallizes with non-*meso* orientations while the spin crossover complex [Fe(5F-sal$_2$333)]BPh$_4$, **2**, crystallizes with a combination of *meso* and non-*meso* orientations disordered over one crystallographic site. Variable temperature electronic absorption spectroscopy of methanolic solutions of **1** and **2** suggests that both are capable of spin state switching in the solution.

Keywords: Fe(III) coordination complexes; hexadentate ligand; Schiff base; spin crossover; UV-Vis spectroscopy; SQUID; EPR spectroscopy

1. Introduction

Spin crossover complexes (SCO) constitute an interesting class of materials exhibiting interconversion between different electronic states by varying temperature or pressure or by light. Many potential applications have been suggested for their use, including their utilization in data storage, sensors, and display technologies. Fe(II) SCO complexes are more studied in the literature in comparison to Fe(III), and spin crossover is observed only very rarely in Mn(III). We have studied the effect of ligand flexibility on spin state choices in both Fe(III) and Mn(III) using some of the families of hexadentate Schiff base ligands of the type shown in Figure 1 [1–6].

Such chelates are formed by a condensation reaction of linear tetra-amines and substituted salicylaldehydes, and our studies to date have focused mostly on complexes from the "222", "323", and "232" series, where the numbers indicate the number of methylene groups connecting adjacent nitrogen atoms. Here, we show the results of our studies into the effect of the longer chain ligand formed from the "333" polyamine on spin state choices in the resultant Fe(III) complexes. The results of our studies into spin state choices with various metal–ligand combinations, including those reported here, are summarized in Table 1.
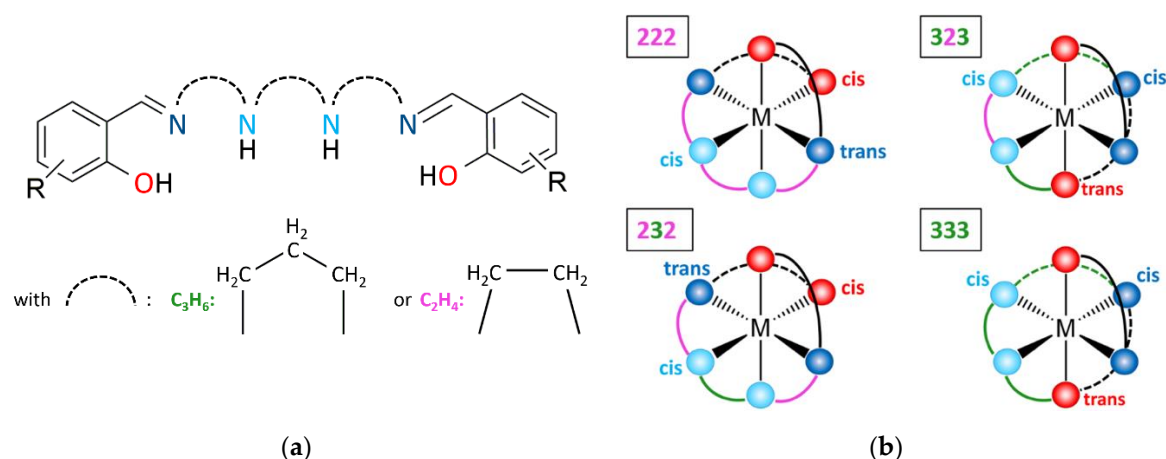
Figure 1. (**a**) Depiction of hexadentate ligands with different chain lengths and (**b**) resulting coordination geometry around a trivalent 3-D metal ion.

Table 1. Donor orientations and spin states for Fe(III) and Mn(III) complexes with selected hexadentate Schiff base ligands. (LS = low spin; HS = high spin; SCO = spin crossover).

Bond Type	R-Sal$_2$-222	R-Sal$_2$-232	R-Sal$_2$-323	R-Sal$_2$-333
O	*cis*	*cis*	*trans*	*trans*
N$_{amine}$	*cis*	*cis*	*cis*	*cis*
N$_{imine}$	*trans*	*trans*	*cis*	*cis*
Mn(III)	HS [3,7]	HS [a]	LS, HS, SCO [1–3,7–13]	HS [14]
Fe(III)	LS, HS, SCO [15–24]	LS, HS, SCO [4,24]	LS [24–26]	HS, SCO [24,25]

[a] G.G. Morgan unpublished results.

In both Fe(III) and Mn(III) complexes, three possible spin arrangements are possible in mononuclear complexes. These comprise the fully spin paired or low spin (LS) arrangement, the fully unpaired or high spin (HS) combination, and a mixture of paired and unpaired, typically termed the intermediate spin (IS) choice. In Fe(III) complexes, these descriptions (LS, IS, and HS) are regularly and accurately used. However, due to the prevalence of the S = 2 HS state in Mn(III), any other spin state was historically considered an oddity and the use of "LS" to describe the S = 1 state became common usage. In Table 1, "LS" is therefore used to describe the S = 1 state as is common in the literature. The true low spin S = 0 state has not yet been observed in any manganese (III) complex. Table 1 summarizes the results of our investigations on spin state choices for Fe(III) and Mn(III) in a range of coordination geometries engineered by binding to the type of N$_4$(O$_2$)$^-$ chelating ligands depicted in Figure 1. The first point to note is that the S = 2 state is dominant for Mn(III) across the four ligand types. However in 2006, our group discovered that the R-Sal$_2$-323 ligand family promoted SCO in Mn(III) [3] and several crystal engineering studies on such complexes followed [1,2,9,11,13]. Although most of these SCO transitions occur below room temperature, some Mn(III) complexes of the R-Sal$_2$-323 ligand family also persist in the *S* = 1 state up to room temperature, and these are defined in Table 1 as LS.

In contrast to manganese, iron (III) shows a range of observed spin states with the four ligand types highlighted in Table 1. It has long been known that the R-Sal$_2$-222 ligand family promotes SCO in iron(III) in addition to stabilizing both HS and LS complexes across a temperature range [15–24]. The Fe(III) R-Sal$_2$-222 complexes have, in recent years, been extensively developed as new switchable materials due to the ease of derivatization which has led to the synthesis of ionic liquids [27], liquid crystals [28], Langmuir-Blodgett film formation with amphiphilic complexes [6,29], and preparation of templated nanowires [21]. We have also observed SCO in Fe(III) complexes from the R-Sal$_2$-232 ligand type [4],

but the majority of this class of compound remains HS from room temperature down to 5 K. In contrast, the R-Sal$_2$-323 ligand type has been shown by Reedjik [26] to promote the LS state in iron (III).

Less is known, however, about the iron (III) spin state preferences that would be conferred by coordination to the R-Sal$_2$-333 ligand type. An early work by Ito and co-workers [25] reported the solid-state and methanolic solution-state properties of the nitrate salts of the iron (III) complexes with R-Sal$_2$-323 and R-Sal$_2$-333 ligands, where R was hydrogen [25]. In the solid state, the iron (III) complex with H-Sal$_2$-323 was LS over the measured range, while that with H-Sal$_2$-323 was HS. Ito also used the Evans' NMR technique and variable temperature electronic absorption spectroscopy to monitor the spin state of both complexes in methanol solution. The LS complex with H-Sal$_2$-323 showed no change in solution, i.e., remained LS with only weak thermochromism in methanol. The HS complex with H-Sal$_2$-333, however, demonstrated a strong temperature dependence as shown by both NMR and UV-Vis absorption and a clear isosbestic point is apparent in the electronic absorption spectra recorded between 268–322 K.

At the outset of this work, the nitrate salt of the Fe(III) complex with H-Sal$_2$-333 reported by Ito in 1983 was the only ferric complex with this ligand type in the literature. Given that SCO for this complex was detected in solution, the R-Sal$_2$-333 ligand type was deemed to constitute a good basis for further investigations into the choice of Fe(III) spin state when coordinated to this ligand type. Here, we report two new Fe(III) complexes with 5-Fluoro-Sal$_2$-333 in two crystalline lattices [Fe(5F-sal$_2$333)]Cl, **1**, and [Fe(5F-sal$_2$333)]BPh$_4$, **2**. Both compounds were examined by single crystal diffraction, and an important and new result to emerge from this study was the variation in orientation of the hydrogen atoms on the two secondary amine nitrogen atoms in the 9-carbon length ligand backbone between non-*meso* (Type A) and a disordered combination of *meso* and non-*meso* co-crystallized on the same site (Type B).

To recall the definition of *meso* and non-*meso* in stereochemistry, there is the special case where a molecule exhibits two stereo centres but is achiral, since one conformation shows an intramolecular C$_s$-symmetry which is then defined as the *meso* form. By using a hexadentate Schiff base ligand formed from condensation of a substituted salicylaldehyde and N,N'-bis(3-aminopropyl)-propylenediamine (333) and by forming the iron (III) complex, the binding amine nitrogen atoms, N2 and N3 (shown in turquoise in Figure 2), can have their attached hydrogen atoms either both pointing in the same direction leading to the *meso* form or in opposite directions, leading to the non-*meso* form. The results of our structural studies into the iron (III) complexes **1** and **2** reveal two structural types (Figure 2): (i) pure non-*meso* (Type A) and (ii) a disordered combination of *meso* and non-*meso*, which co-crystallize on the same Fe site (Type B).

non-*meso*　　　　　　　　*meso*　　　　　　　mixed *meso*/non-*meso*
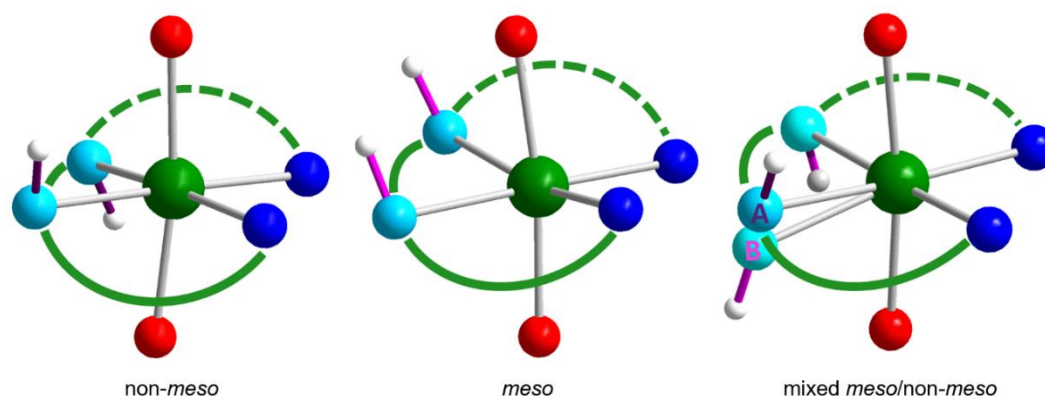
Figure 2. Hydrogen atoms at the amine nitrogen of the R-Sal$_2$333 backbone, forming the non-*meso* Type A form (**Left**) and *meso* form (**Middle**) of the ligand. Co-crystallization of both modes (**Right**) was observed in the tetraphenylborate complex **2** and this crystallization mode was termed Type B.

2. Materials and Methods

2.1. Materials and Instrumentation

All chemicals used were supplied as described: N,N'-Bis-(3-aminopropyl)-1,3-propandiamine (Sigma-Aldrich, 90%), 5-fluorosalicylaldehyde (Fluorochem, 98%), iron (III) chloride hexahydrate (Sigma-Aldrich, 97%), sodium tetraphenylborate (Sigma-Aldrich, $\geq$ 99.5%), acetonitrile (Fisher Scientific, 99.8%), and ethanol (Fisher Scientific, $\geq$ 99.5%). Elemental analysis was recorded on an Exeter Analytical CE-440 CHN analyzer, for Carbon, Hydrogen, and Nitrogen. Infrared spectra were recorded using a Bruker Alpha Platinum attenuated total reflection (ATR) spectrometer. Mass spectrometry was recorded using a Waters 2695 separations module electrospray spectrometer on acetonitrile solutions of **1** and **2**.

2.2. Synthesis

The synthesis of compounds **1** and **2** is straightforward, and the complexes were recovered in varying yields. Solid 5-fluorosalicylaldehyde (1.0 mmol) was added to a solution of N,N'-bis(3-aminopropyl)-1,3-propandiamine (0.5 mmol) in 50:50 ethanol/acetonitrile (15 mL), causing a yellow color to form. After stirring for 15 min, solid iron (III) chloride hexahydrate (0.5 mmol) was added whereupon the solution turned dark black. For synthesis of complex **2**, solid sodium tetraphenylborate (0.5 mmol) was then added. For both complexes **1** and **2**, the dark solution was stirred at room temperature for 30 min, then gravity filtered and allowed to stand for slow evaporation for 3–4 days. Dark purple crystals were collected for both compounds **1** (*ca.* 15%) and **2** (*ca.* 20%) which were suitable for single crystal X-ray structural analysis.

Complex **1**, [Fe(5F-sal$_2$333)]Cl: Elemental analysis calculated for $C_{23}H_{28}N_4O_2F_2ClFe$. Calculated: C 52.94, H 5.41, and N 10.74. Found: C 52.86, H 5.37, and N 10.72. Mass Spec: 486.33 ES$^+$.

Complex **2**, [Fe(5F-sal$_2$333)]BPh$_4$: Elemental analysis calculated for $C_{47}H_{48}BN_4O_2F_2Fe$. Calculated: C 67.33, H 5.77, and N 6.68. Found: C 67.10, H 5.75, and N 6.57. Mass Spec: 519.24 ES$^+$.

2.3. Single-Crystal X-Ray Structure Determinations

X-ray crystallography was carried out on suitable single crystals using an Oxford Supernova diffractometer (Oxford Instruments, Oxford, United Kingdom). Datasets were measured using monochromatic Cu-Kα and Mo-Kα radiation for **1** and **2** respectively and corrected for absorption. The temperature was controlled with an Oxford Cryosystem instrument. A complete dataset was collected, assuming that the Friedel pairs are not equivalent. An analytical absorption correction based on the shape of the crystal was performed [30]. All structures were solved by dual-space direct methods (SHELXT) [31] and refined by full matrix least-squares on F^2 for all data using SHELXL-2016 [31]. The hydrogen atoms attached to nitrogen were located in the difference Fourier map and allowed to refine freely. All other hydrogen atoms were added at calculated positions and refined using a riding model. Their isotropic displacement parameters were fixed to 1.2 times the equivalent one of the parent atom. Anisotropic displacement parameters were used for all non-hydrogen atoms. Crystallographic details for both compounds are summarized in Table A1 (Appendix A) and crystallographic data for the structures reported in this paper have been deposited with the Cambridge Crystallographic Data Centre as supplementary publication numbers CCDC-1884365 (1, 100 K), CCDC-1884366 (2, 100 K), and CCDC-1884367 (2, 293 K).

2.4. Magnetic Measurements

The magnetic susceptibility measurements were obtained using a Quantum Design Magnetic Property Measurement System, the MPMS-XL SQUID Magnetometer (Quantum Design, San Diego, CA, USA) operating between 5 and 300 K. Direct current (DC) measurements were performed on a polycrystalline sample of 11.1 mg of complex **1** and of 11.9 mg of complex **2**. Each sample was wrapped in a polyethylene membrane, and susceptibility data were collected at 0.1 T between 5–300 K

in cooling and warming mode. The magnetization data was collected at 100 K in order to check for ferromagnetic impurities, which were found to be absent in the samples. Diamagnetic corrections were applied to correct for contribution from the sample holder, and the inherent diamagnetism of the sample was estimated with the use of Pascal's constants.

2.5. UV-Vis and Electron Paramagnetic Resonance (EPR) Spectroscopy

UV-Vis solution spectra of [Fe(5F-sal$_2$333)]Cl, **1**, and [Fe(5F-sal$_2$333)]BPh$_4$, **2**, were recorded on an Agilent UV-Vis spectrometer fitted with an Oxford Instruments cryostat insert. Solid state variable temperature EPR spectra were recorded on a Magnettech X-band EPR spectrometer (Freiberg Instruments, Freiberg, Germany) (9.430 GHz) at variable temperatures. A modulation amplitude of 0.7 mT was used in conjunction with a microwave power of 0.1 mW and a gain of 10.

3. Results

3.1. Synthetic Route

Synthesis of [Fe(5F-sal$_2$333)]Cl, **1**, and [Fe(5F-sal$_2$333)]BPh$_4$, **2**, was achieved in a facile reaction by condensation of N,N'-bis(3-aminopropyl)-1,3-propanediamine (333) with two equivalents of 5-fluorosalicylaldehyde followed by addition of hydrated iron (III) chloride (complex **1**) with further addition of sodium tetraphenylborate in the case of complex **2**, Scheme 1. The filtered reaction mixture on slow evaporation yielded complexes **1** and **2** as dark purple crystals.
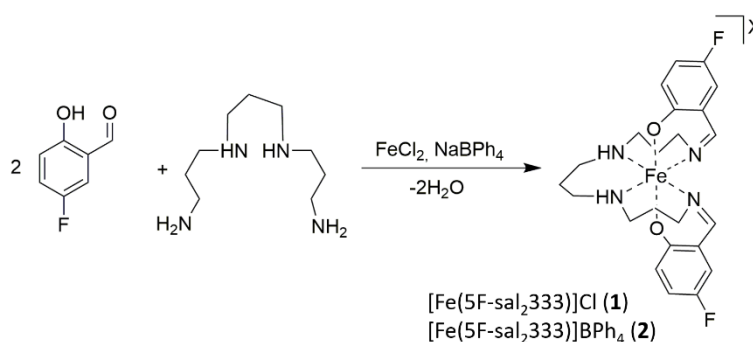
**Scheme 1.** Synthesis of [Fe(F-Sal$_2$333)]X complex series **1** and **2**.

Both complexes were characterized by mass spectrometry, elemental analysis, IR spectroscopy, single crystal diffraction, and SQUID magnetometry. Both showed a characteristic C=N stretch at 1611 cm^{-1}, confirming formation of the Schiff base and a resonance at 3051 cm^{-1} in the case of **2** and confirming the anion methathesis to the tetraphenylborate counterion. Elemental analysis confirmed the purity of both crystalline samples.

3.2. Structural Analysis

For crystallographic details for complexes **1** and **2**, see Table A1 (Appendix A). Complex **1** crystallized in orthorhombic and non-centrosymmetric space group *Pccn* where the asymmetric unit comprises half of one complex [FeL]$^+$ cation and half of one chloride counterion. The two halves of the complex cation are related by a C2 axis which passes through the central carbon of the middle propylene chain on the ligand backbone. The well-ordered non-*meso* arrangement of the amine on N2 is illustrated in Figure 3.

The chloride counterion within the crystal lattice exhibits short contacts to the hydrogen atoms of the amine nitrogen atoms of the ligand backbone, which leads to the formation of a 1D-chain, Figure 4. Bond length data at 100 K are in line with an S = 5/2 spin state assignment at this temperature as the three bond types, Fe-O$_{phenolate}$ (1.9426(9) Å), Fe-N$_{imine}$ (2.1398(11) Å), and Fe-N$_{amine}$ (2.1837(11) Å) are all typical for the HS state with these types of donor [21].

| (**a**) | (**b**) | (**c**) |
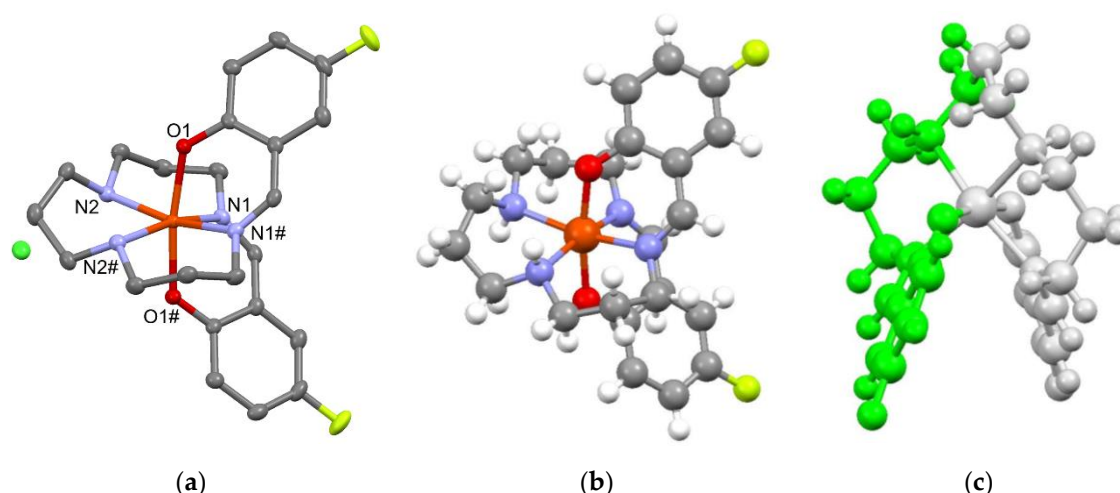
Figure 3. (**a**) View of [Fe(5F-sal₂333)]Cl, complex **1**, showing symmetry equivalence of donor atoms related by the central C2 axis, (**b**) view of the complex cation showing the orientation of hydrogen atoms, including the non-*meso* arrangement of amine hydrogens, and (**c**) depiction of the symmetry relationship of the two halves of the complex.
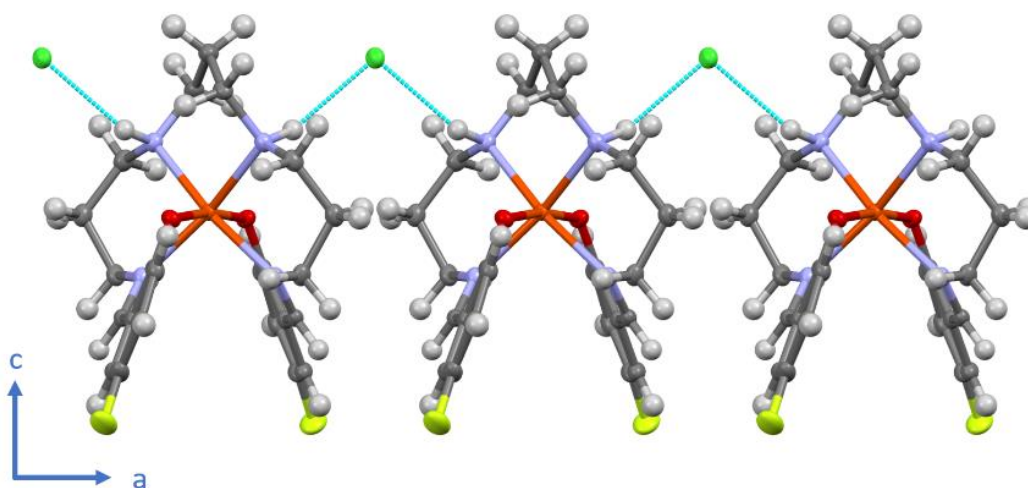

Figure 4. View of 1-D hydrogen bonding chain between adjacent complexes, mediated by chloride counterions in [Fe(5F-sal₂333)]Cl, **1**.

Complex **2**, [Fe(5F-sal₂333)]BPh₄, crystallizes in triclinic space group P-1 where the asymmetric unit at 100 K comprises one full occupancy disordered [FeL]⁺ cation and one full occupancy well-ordered BPh₄⁻ anion, Figure 5. Both the *meso* and non-*meso* orientations of the amine hydrogens co-crystallize on a single site leading to the disorder of most of the nine propylene carbons and one of the amine nitrogen atoms over two positions. Each component of the disorder was modelled separately within the crystal structure, and the *meso* and non-*meso* orientations of the hydrogen atoms on both amine nitrogen positions co-crystallized on single site are clear, Figure 5.

Structural data for complex **2** was collected initially at 100 K and some months later at 293 K on a different crystal, after analysis of the SQUID data which revealed the change in spin state between the two temperatures. Bond length data, Table 2, indicate a LS state at 100 K with markedly shorter bond lengths for the three bond types, Fe-O$_\text{phenolate}$ (*ca.* 1.86 Å), Fe-N$_\text{imine}$ (*ca.* 1.95 Å), and Fe-N$_\text{amine}$ (with disorder component *ca.* 2–2.10 Å) than those for HS complex **1** at the same temperature. The bond lengths for **1** at 100 K are in line with other LS complexes with comparable donors [21]. At 293 K SQUID data for **2** indicate a small HS fraction, and this is reflected in the small increase in bond

lengths compared with those at 100 K: Fe-O$_{phenolate}$ (*ca.* 1.87) Å), Fe-N$_{imine}$ (*ca.* 1.97 Å), and Fe-N$_{amine}$ (with disorder component *ca.* 2–2.15 Å), suggesting that the majority of sites remain LS. The absence of hydrogen bond donors or acceptors on the BPh$_4^-$ counterions and the large distance between the complex cations means no hydrogen bond network emerges to tether the complexes together as was the case with the fully HS analogue, complex **1**. The absence of hydrogen bonding in complex **2** may contribute to the different spin state choices in the two complexes.


|(**a**)|(**b**)|(**c**)|
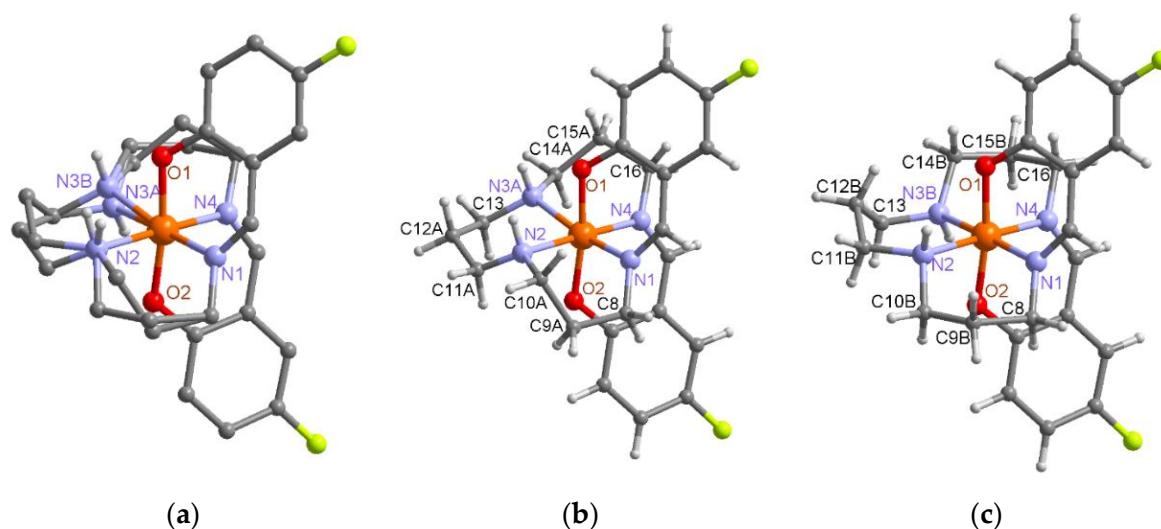
Figure 5. View of asymmetric unit of [Fe(5F-sal$_2$333)]BPh$_4$, **2**, showing (**a**) disorder of three propylene groups in ligand backbone due to co-crystallization of *meso* and non-*meso* forms; view of (**b**) the *meso* form and (**c**) the pure non-*meso* orientation.

Table 2. Bond length data for complexes **1** and **2**.

	[Fe(5F-sal$_2$333)]Cl (1) 100 K	Fe-Donor	[Fe(5F-sal$_2$333)]BPh$_4$ (2) 100 K	[Fe(5F-sal$_2$333)]BPh$_4$ (2) 293 K
Fe-O$_{phenolate}$	1.9426(9)	Fe–O(2)	1.8521(14)	1.8569(15)
		Fe–O(1)	1.8721(15)	1.8801(16)
Fe-N$_{imine}$	2.1398(11)	Fe–N(1)	1.9480(15)	1.9667(18)
		Fe–N(4)	1.9582(14)	1.9778(16)
Fe-N$_{amine}$	2.1837(11)	Fe–N(3A)	2.014(3)	2.017(5)
		Fe–N(2)	2.0624(16)	2.0734(19)
		Fe–N(3B)	2.134(4)	2.162(7)

### 3.3. Magnetic Characterization

Magnetic susceptibility of complexes **1** and **2** were recorded on an MPMS-XL magnetometer between 5–300 K in warming and cooling modes. The expected $\chi_M T$ values for S = 5/2 and S = 1/2 are 4.25 and 0.375 cm^3 K/mol respectively, and plots of $\chi_M T$ versus *T*, Figure 6, indicate that complex **1** remains HS over the measured temperature range. Complex **2** persists in the predominantly LS state on warming from 5 K to around 250 K above which the $\chi_M T$ value starts to rise, indicating some thermal population of the HS state.
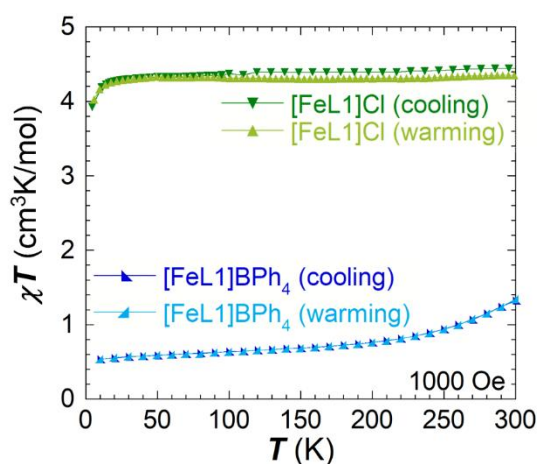
Figure 6. Plots of $\chi_M T$ versus T for complexes **1** (green) and **2** (blue) between 5–300 K in cooling and warming mode.

3.4. Solid State EPR Spectroscopy

Solid state variable temperature EPR spectra of complexes **1** and **2** were recorded on a Magnettech X-band EPR spectrometer, Figure 7. Complex **1** shows the characteristic broad S = 5/2 with g = 2 over the whole temperature range which fits well with the HS assignment from SQUID magnetometry. The EPR spectra of complex **2**, [Fe(5F-sal$_2$333)]BPh$_4$, are also in line with the SQUID data, showing a gradual thermal SCO in the solid state. A characteristic S = 1/2 signal at g = 2 with differentiation of the *x*, *y*, and *z* components is apparent at low temperatures for complex **2**, which is diminished on warming to 353 K.
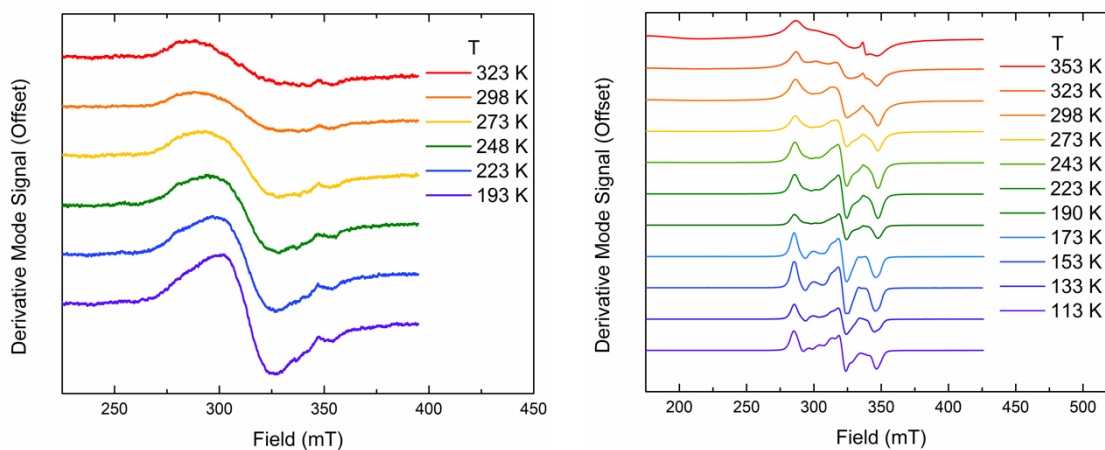

Figure 7. Variable temperature EPR spectra of complex **1** (**left**) and **2** (**right**) at variable temperature.

3.5. UV-Vis Solution Studies

It was also possible to collect solution state variable temperature electronic absorption for complexes **1** and **2** in methanol, Figure 8, using an Oxford Instruments cryostat insert for a benchtop UV-Vis spectrometer using a 1.0×10^{-4} mol/L methanolic solution of **1** and 1.46×10^{-4} mol/L methanolic solution of **2**. The spectra suggest that thermal SCO could be achieved in both complexes in this medium despite the fixed HS moment observed between 5–300 K in the crystalline form of complex **1**. The spectra of both complexes show two broad absorptions at around 380 and 620 nm; the latter of which were attributed to charge transfer absorptions rather than d-d transitions. The higher energy band is likely due to ligand only transitions. A strong similarity between the electronic spectra of **1** and **2** in solution is to be expected given that the cation is identical in each. It is also to be expected that the fixed *meso*/non-*meso*

differences arise in the solid state due to significant differences in packing between the two variously sized anions. In solution, it is most likely that the complex cation may be in a dynamic exchange between the two forms, and therefore, the spectra of **1** and **2** in methanol should be similar. The higher energy band at 380 nm grows on cooling for both compounds while that at 620 nm narrows on cooling, suggesting population of the LS state which has a narrower vibrational energy well.

(**a**)   (**b**)
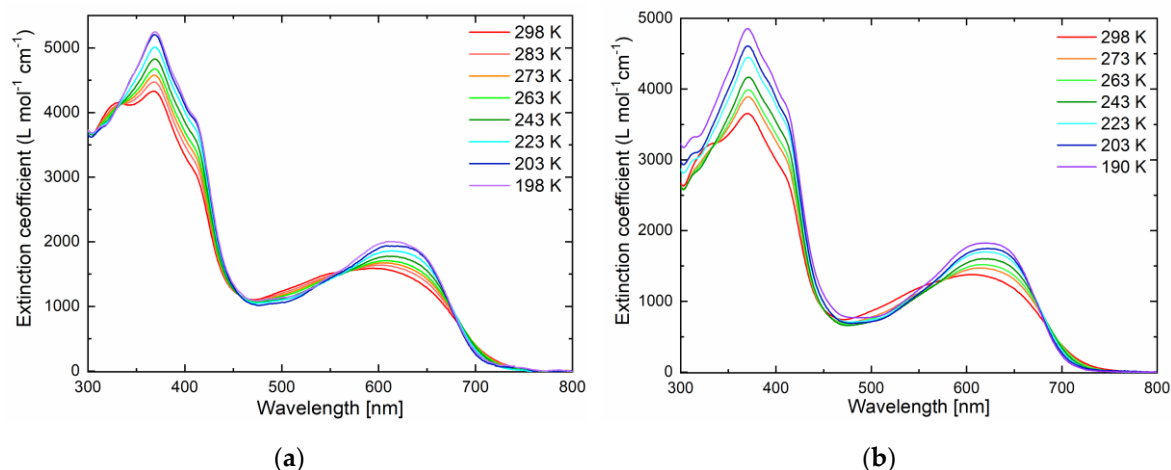
Figure 8. Variable temperature UV-Vis characterization of complex **1** (**a**) and **2** (**b**).

4. Discussion

In this work, we have investigated the influence of geometry and counterion effects in determining the spin state choices in an iron (III) complex with the 5-Fluoro-sal$_2$333 ligand in a Cl^- or BPh_4^- lattice. In the solid state the $[Fe(5F\text{-}sal_2333)]^+$ complex adopts the $S = 5/2$ spin state in a chloride lattice and the $S = \frac{1}{2}$ spin state in the tetraphenylborate lattice. The BPh_4^- complex shows onset of a gradual spin crossover on warming from 5 K, but it is still mainly in the LS state by room temperature. An interesting result to emerge from the investigation was the observation that there were two possible orientations (*meso* and non-*meso*) for the hydrogen atoms on the amine nitrogen donors and that a magnetostructural correlation may be present. Complex **1**, which adopted the pure non-*meso* form, showed a preference for the HS state while complex **2,** which crystallized as a mixture of *meso* and non-*meso*, showed preference for the LS state with onset of a gradual SCO only above 250 K. In conclusion, we have established that R-sal$_2$333 ligands can promote SCO in Fe(III) both in the solid state and in solution. Moreover, we have shown that a new type of ligand distortion (*meso*/non-*meso*) exists that may affect the spin state choice and profile of the spin crossover thermal evolution. Future work will include detailed Mössbauer spectroscopy on existing samples reported here and preparation and characterization of further members of the series.

Appendix A

Table A1. Crystallographic details for complexes **1** and **2**.

Compound	[Fe(5F-sal$_2$333)]Cl (1)	[Fe(5F-sal$_2$333)]BPh$_4$ (2)	[Fe(5F-sal$_2$333)]BPh$_4$ (2)
Empirical formula	C$_{23}$H$_{28}$N$_4$O$_2$F$_2$ClFe	C$_{47}$H$_{48}$BN$_4$O$_2$F$_2$Fe	C$_{47}$H$_{48}$BN$_4$O$_2$F$_2$Fe
Formula weight	521.79	805.55	805.55
Crystal system	orthorhombic	triclinic	triclinic
Space group	*Pccn*	*P−1*	*P−1*
Crystal size (nm)	0.195 × 0.114 × 0.033	0.3335 × 0.2632 × 0.2017	0.405 × 0.350 × 0.337
a (Å)	7.39810(6)	10.7385(2)	10.80774(8)
b (Å)	16.3083(2)	13.9687(3)	14.0136(1)
c (Å)	18.6359(2)	14.7851(2)	14.9232(2)
α (°)	90	102.984(2)	103.0383(7)
β (°)	90	94.039(1)	94.2739(6)
γ (°)	90	109.415(2)	107.6673(7)
V (Å^3)	2248.43(4)	2012.64(6)	2073.03(4)
Z	4	2	2
d$_{calc}$ (g cm^{-3})	1.541	1.329	1.291
T (K)	100(2)	100(2)	293(2)
μ (mm^{-1})	6.871	0.429	0.416
F(000)	1084	846	846
Limiting indices	h = ± 9, k = ± 20, l = ± 23	h = ± 13, k = ± 17, l = ± 8	h = ± 13, k = ± 17, l = ± 18
Reflections collected/unique	21831/2378	35866/8833	79115/7853
R(int)	0.0288	0.0315	0.0191
Completeness to Θ (%)	99.7	99.5	99.7
Data/restraints/parameters	2378/0/151	8833/0/578	7853/0/578
GooF on F^2	1.047	1.041	1.079
Final R indices (I > 2σ (I))	R$_1$ = 0.0274, wR$_2$ = 0.0760	R$_1$ = 0.0414, wR$_2$ = 0.0928	R$_1$ = 0.0396, wR$_2$ = 0.1068
R indices (all data)	R$_1$ = 0.0292, wR$_2$ = 0.0777	R$_1$ = 0.0479, wR$_2$ = 0.0963	R$_1$ = 0.0420, wR$_2$ = 0.1085
Largest diff. peak/hole (e$^-$Å^{-3})	0.255 and −0.457	0.332 and −0.723	0.292 and −0.584
CCDC no.	1884365	1884366	1884367

References

1.　Martinho, P.N.; Gildea, B.; Harris, M.M.; Lemma, T.; Naik, A.D.; Müller-Bunz, H.; Keyes, T.E.; Garcia, Y.; Morgan, G.G. Cooperative Spin Transition in a Mononuclear Manganese(III) Complex. *Angew. Chem. Int. Ed.* **2012**, *51*, 12597–12601. [CrossRef] [PubMed]

2.　Gildea, B.; Harris, M.M.; Gavin, L.C.; Murray, C.A.; Ortin, Y.; Müller-Bunz, H.; Harding, C.J.; Lan, Y.; Powell, A.K.; Morgan, G.G. Substituent Effects on Spin State in a Series of Mononuclear Manganese(III) Complexes with Hexadentate Schiff-Base Ligands. *Inorg. Chem.* **2014**, *53*, 6022–6033. [CrossRef] [PubMed]

3.　Morgan, G.G.; Murnaghan, K.D.; Müller-Bunz, H.; McKee, V.; Harding, C.J. A Manganese(III) Complex That Exhibits Spin Crossover Triggered by Geometric Tuning. *Angew. Chem. Int. Ed.* **2006**, *45*, 7192–7195. [CrossRef] [PubMed]

4.　Griffin, M.; Shakespeare, S.; Shepherd, H.J.; Harding, C.J.; Létard, J.F.; Desplanches, C.; Goeta, A.E.; Howard, J.A.K.; Powell, A.K.; Mereacre, V.; et al. A Symmetry-Breaking Spin-State Transition in Iron(III). *Angew. Chem. Int. Ed.* **2011**, *50*, 896–900. [CrossRef] [PubMed]

5.　Murray, C.; Gildea, B.; Müller-Bunz, H.; Harding, C.J.; Morgan, G.G. Co-Crystallisation of Competing Structural Modes in Geometrically Constrained Jahn–Teller Manganese(III) Complexes. *Dalton Trans.* **2012**, *41*, 14487–14489. [CrossRef] [PubMed]

6.　Martinho, P.N.; Kühne, I.A.; Gildea, B.; McKerr, G.; O'Hagan, B.; Keyes, T.E.; Lemma, T.; Gandolfi, C.; Albrecht, M.; Morgan, G.G. Self-Assembly Properties of Amphiphilic Iron(III) Spin Crossover Complexes in Water and at the Air–Water Interface. *Magnetochemistry* **2018**, *4*, 49. [CrossRef]

7.　Gandolfi, C.; Cotting, T.; Martinho, P.N.; Sereda, O.; Neels, A.; Morgan, G.G.; Albrecht, M. Synthesis and Self-Assembly of Spin-Labile and Redox-Active Manganese(III) Complexes. *Dalton Trans.* **2011**, *40*, 1855–1865. [CrossRef] [PubMed]

8.　Wang, S.; Ferbinteanu, M.; Marinescu, C.; Dobrinescu, A.; Ling, Q.-D.; Huang, W. Case Study on a Rare Effect: The Experimental and Theoretical Analysis of a Manganese(III) Spin-Crossover System. *Inorg. Chem.* **2010**, *49*, 9839–9851. [CrossRef]

9. Gildea, B.; Gavin, L.C.; Murray, C.A.; Müller-Bunz, H.; Harding, C.J.; Morgan, G.G. Supramolecular Modulation of Spin Crossover Profile in Manganese(III). *Supramol. Chem.* **2012**, *24*, 641–653. [CrossRef]

10. Wang, S.; Xu, W.-T.; He, W.-R.; Takaishi, S.; Li, Y.-H.; Yamashita, M.; Huang, W. Structural Insights into the Counterion Effects on the Manganese(III) Spin Crossover System with Hexadentate Schiff-base Ligands. *Dalton Trans.* **2016**, *45*, 5676–5688. [CrossRef]

11. Fitzpatrick, A.J.; Trzop, E.; Müller-Bunz, H.; Dîrtu, M.M.; Garcia, Y.; Collet, E.; Morgan, G.G. Electronic vs. Structural Ordering in a Manganese(III) Spin Crossover Complex. *Chem. Commun.* **2015**, *51*, 17540–17543. [CrossRef] [PubMed]

12. Fitzpatrick, A.J.; Stepanovic, S.; Müller-Bunz, H.; Gruden-Pavlović, M.A.; García-Fernández, P.; Morgan, G.G. Challenges in Assignment of Orbital Populations in a High Spin Manganese(III) Complex. *Dalton Trans.* **2016**, *45*, 6702–6708. [CrossRef] [PubMed]

13. Pandurangan, K.; Gildea, B.; Murray, C.; Harding, C.J.; Müller-Bunz, H.; Morgan, G.G. Lattice Effects on the Spin-Crossover Profile of a Mononuclear Manganese(III) Cation. *Chem. Eur. J.* **2012**, *18*, 2021–2029. [CrossRef] [PubMed]

14. Wang, S.; He, W.-R.; Ferbinteanu, M.; Li, Y.-H.; Huang, W. Tetragonally Compressed High-Spin Mn(III) Schiff Base Complex: Synthesis, Crystal Structure, Magnetic Properties and Theoretical Calculations. *Polyhedron* **2013**, *52*, 1199–1205. [CrossRef]

15. Floquet, S.; Carmen Muñoz, M.; Rivière, E.; Clément, R.; Audière, J.-P.; Boillot, M.-L. Structural Effects on the Magnetic Properties of Ferric Complexes in Molecular Materials or a Lamellar $CdPS_3$ Host Matrix. *New J. Chem.* **2004**, *28*, 535–541. [CrossRef]

16. Pritchard, R.; Barrett, S.A.; Kilner, C.A.; Halcrow, M.A. The Influence of Ligand Conformation on the Thermal Spin Transitions in Iron(III) Saltrien Complexes. *Dalton Trans.* **2008**, 3159–3168. [CrossRef] [PubMed]

17. Nishida, Y.; Kino, K.; Kida, S. X-Ray structural study of [Fe(saltrien)]X (X = Br·$2H_2O$, BPh_4 or PF_6). Origin of Unusual Magnetic Behaviour of the Spin-Crossover Complex [Fe(saltrien)]PF_6. *J. Chem. Soc. Dalton Trans.* **1987**, 1957–1961. [CrossRef]

18. Sinn, E.; Sim, G.; Dose, E.V.; Tweedle, M.F.; Wilson, L.J. Iron(III) Chelates with Hexadentate Ligands from Triethylenetetramine and b-diketones or Salicylaldehyde. Spin State Dependent Crystal and Molecular Structures of [Fe(acac)$_2$trien]PF_6 (S = 5/2), [Fe(acacCl)$_2$trien]PF_6 (S = 5/2), [Fe(sal)$_2$trien]Cl·$2H_2O$ (S = 1/2). *J. Am. Chem. Soc.* **1978**, *100*, 3375–3390. [CrossRef]

19. Martinho, P.N.; Harding, C.J.; Müller-Bunz, H.; Albrecht, M.; Morgan, G.G. Inducing Spin Crossover in Amphiphilic Iron(III) Complexes. *Eur. J. Inorg. Chem.* **2010**, *2010*, 675–679. [CrossRef]

20. Gandolfi, C.; Moitzi, C.; Schurtenberger, P.; Morgan, G.G.; Albrecht, M. Improved Cooperativity of Spin-Labile Iron(III) Centers by Self-Assembly in Solution. *J. Am. Chem. Soc.* **2008**, *130*, 14434–14435. [CrossRef] [PubMed]

21. Martinho, P.N.; Lemma, T.; Gildea, B.; Picardi, G.; Müller-Bunz, H.; Forster, R.J.; Keyes, T.E.; Redmond, G.; Morgan, G.G. Template Assembly of Spin Crossover One-Dimensional Nanowires. *Angew. Chem. Int. Ed.* **2012**, *51*, 11995–11999. [CrossRef] [PubMed]

22. Vieira, B.J.C.; Coutinho, J.T.; Santos, I.C.; Pereira, L.C.J.; Waerenborgh, J.C.; da Gama, V. [Fe(nsal$_2$trien)]SCN, a New Two-Step Iron(III) Spin Crossover Compound, with Symmetry Breaking Spin-State Transition and an Intermediate Ordered State. *Inorg. Chem.* **2013**, *52*, 3845–3850. [CrossRef]

23. Nemec, I.; Herchel, R.; Šalitroš, I.; Trávníček, Z.; Moncol, J.; Fuess, H.; Ruben, M.; Linert, W. Anion Driven Modulation of Magnetic Intermolecular Interactions and Spin Crossover Properties in an Isomorphous Series of Mononuclear Iron(III) Complexes with a Hexadentate Schiff Base Ligand. *CrystEngComm* **2012**, *14*, 7015–7024. [CrossRef]

24. Hayami, S.; Matoba, T.; Nomiyama, S.; Kojima, T.; Osaki, S.; Maeda, Y. Structures and Magnetic Properties of Some Fe(III) Complexes with Hexadentate Ligands: In Connection with Spin-Crossover Behavior. *Bull. Chem. Soc. Jpn.* **1997**, *70*, 3001–3009. [CrossRef]

25. Ito, T.; Sugimoto, M.; Ito, H.; Toriumi, K.; Nakayama, H.; Mori, W.; Sekizaki, M. A Chelate Ring Size Effect on Spin States of Iron(III) Complexes with Hexadentate Ligands Derived from Salicylaldehyde and 4,8-Diazaundecane-1,11-diamine(3,3,3-tet) or 4,7-Diazadecane-1,10-diamine(3,2,3-tet), and their X-Ray Structures. *Chem. Lett.* **1983**, *12*, 121–124. [CrossRef]

26. Kannappan, R.; Tanase, S.; Mutikainen, I.; Turpeinen, U.; Reedijk, J. Low-Spin Iron(III) Schiff-Base Complexes with Symmetric Hexadentate Ligands: Synthesis, Crystal Structure, Spectroscopic and Magnetic Properties. *Polyhedron* **2006**, *25*, 1646–1654. [CrossRef]

27. Fitzpatrick, A.J.; O'Connor, H.M.; Morgan, G.G. A Room Temperature Spin Crossover Ionic Liquid. *Dalton Trans.* **2015**, *44*, 20839–20842. [CrossRef]

28. Seredyuk, M.; Gaspar, A.B.; Ksenofontov, V.; Galyametdinov, Y.; Verdaguer, M.; Villain, F.; Gütlich, P. Spin-Crossover and Liquid Crystal Properties in 2D cyanide-bridged Fe^{II}-$M^{I/II}$ Metalorganic Frameworks. *Inorg. Chem.* **2010**, *49*, 10022–10031. [CrossRef]

29. Soyer, H.; Mingotaud, C.; Boillot, M.-L.; Delhaes, P. Spin Crossover of a Langmuir−Blodgett Film Based on an Amphiphilic Iron(II) Complex. *Langmuir* **1998**, *14*, 5890–5895. [CrossRef]

30. Clark, R.C.; Reid, J.S. The Analytical Calculation of Absorption in Multifaceted Crystals. *Acta Crystallogr. Sect. A* **1995**, *51*, 887–897. [CrossRef]

31. Sheldrick, G.M. Crystal Structure Refinement with SHELXL. *Acta Crystallogr. Sect. C Struct. Chem.* **2015**, *71*, 3–8. [CrossRef] [PubMed]